J. Fluid Mech. (1998), *vol.* 356, *pp.* 125–147. Printed in the United Kingdom

The effect of a two-dimensional cascade of thin streamwise plates on homogeneous turbulence

By J. M. R. GRAHAM

Department of Aeronautics, Imperial College, London SW7 2BY, UK

(Received 26 September 1996 and in revised form 5 September 1997)

An analysis is given, based on rapid distortion theory, of the effect on homogeneous turbulence when it passes through a linear cascade of thin flat plates or aerofoils and in particular the turbulence that emerges on the downstream side. The main results are evaluated for the limiting case in which the spacing ratio of the cascade is very small so that the cascade tends to completely suppress the normal component of velocity of the turbulence everywhere, both within the cascade and downstream of it, resulting in a 'planar' (quasi-two-dimensional) turbulence. Some comparisons with experimental measurements of grid generated turbulence passed through cascades of thin aerofoils and in the regions adjacent to the wakes of isolated streamwise plates in a wind tunnel are shown.

1. Introduction

Rapid distortion theory (RDT) in which the nonlinear and viscous components are neglected in the calculation of changes to a turbulent flow, has been used with some success for a number of cases where the mean strain field which distorts the turbulence is applied rapidly and both it and the boundary conditions on the flow are fairly simple. Examples are the cases analysed by Batchelor & Proudman (1954): one-dimensional strain, no boundaries; Hunt (1973): two-dimensional strain, circular boundary; and Hunt & Graham (1978): suddenly applied blocking by a plain boundary.

Conditions which must be satisfied for RDT to apply to convected turbulence are:

(i) $(u'_\infty/U_\infty)\, l/L_\infty \ll 1$.

(ii) high-turbulence Reynolds number: $Re_T = u'_\infty L_\infty/\nu \gg 1$. Here u'_∞ is a characteristic velocity scale of the turbulence, for example the incident r.m.s. fluctuating streamwise component, L_∞ a lengthscale of the turbulence such as the integral lengthscale, l a lengthscale of the mean strain field, usually a body lengthscale and U_∞ the mean velocity of the free stream. Condition (i) specifies that the mean strain field applied to the turbulence by, for example, a change in the boundary conditions encountered by the flow should be applied sufficiently rapidly. This requirement is that:

(iii) $T_S/T_\infty \ll 1$, where T_S is the time over which the strain is applied and T_∞ is the turnover timescale of the turbulence, L_∞/u'_∞. In the case of convected turbulence, as considered here, this implies that the product: $(x_1/L_\infty)\cdot(u'_\infty/U_\infty) \ll 1$, where x_1 is the downstream distance from the point of first encounter of the mean strain field by the turbulence to the point at which the distorted turbulence field is to be evaluated. For weak turbulence ($u'_\infty/U_\infty \ll 1$), as assumed here, this condition allows x_1 to be of order L_∞, but not $\gg L_\infty$. Recent studies by Perot & Moin (1995) using direct simulation and by Aronson, Johansson & Loefdahl (1997) using wind-tunnel measurement of shear-free turbulence suddenly blocked by a plane streamwise boundary have shown that the convective downstream distance x_1 (or time) within which RDT gives reasonable

agreement with the actual distortion that occurs, corresponds to about one integral lengthscale L_∞ from the leading edge (or onset) of the blocking boundary. However the suppression of the transverse component of the turbulence normal to the boundary continues to be reasonably predicted for a much longer streamwise distance (or time).

In the present paper we are interested in the effect on turbulence passing through a linear cascade of thin flat plates and the form of the turbulence which emerges on the downstream side. The analysis follows closely that of Hunt & Graham (1978, hereinafter referred to as HG) for turbulence suddenly brought into contact with a plain boundary. The analysis was based on RDT and the turbulence was presumed to encounter a long plane wall which had the property of imposing, principally, a zero normal boundary condition on the turbulence without imposing a mean shear. HG also considered the effect of a zero tangential velocity wall boundary condition on the turbulence. The Stokes layer analysis for cases where it is applicable demonstrates an effect which is confined to a region next to the wall of thickness

$$O\{L_\infty[x_1/(L_\infty\, Re_T)]^{1/2}\}.$$

With the above assumptions and with sufficiently high Reynolds number either the Stokes layer or any mean flow boundary layer at x_1/L_∞ not $\gg 1$ can be made thin enough compared to the 'source' layer to be neglected.

The process of turbulence encountering a plane wall can be realized approximately in a number of ways, none of which are uncontroversially representative of this application of RDT. The main comparisons made in HG were with measurements of turbulence adjacent to a moving belt (Thomas & Hancock 1977) in order to remove as far as possible the effects of mean shear at the boundary. The incident turbulence was generated in the usual way by a biplanar grid abutting the walls of the wind tunnel. The layer of incident turbulence which evolved under the influence of the wind tunnel wall and the mean shear of the boundary layer on it was then removed by suction some way downstream of the grid bringing a new unsheared and unconstrained stream of turbulence down onto the moving belt. In this way an approximately shear-free turbulent layer was generated at the expense of some unquantified mean strain field effect at the suction slot. A number of experiments of this type have been undertaken, the first by Uzkan & Reynolds (1967) and the most recent by Aronson *et al.* (1997). Comparisons between theory and experiment were also described in HG for another geometry. The measurements of the normal component of Reynolds stress were made for grid turbulence incident on a long thin flat streamwise plate in the middle of the flow with its leading edge well downstream of the grid (Graham 1975). Both mean and fluctuating shear layers were present, therefore, in this case, but in the region of the measurements they were thin compared to the lengthscale of the turbulence and therefore the thickness of the main blockage layer. Both types of experimental realization, assuming that they achieved what was intended (and both types of flow may be subject to quite significant undesired effects at the 'leading edge'), involve a rapid application of a new zero normal velocity boundary condition to the turbulence field. Even if the change of boundary condition may be considered to be applied instantaneously, as shown in HG Appendix A, the turbulence flow field for these convective flows is inhomogeneous in the streamwise direction over a distance of order L_∞. This is the region within which there is a significant pressure field associated with the interaction between the turbulence and the leading edge. The simplified theory given for the infinite plane wall can only be applied downstream of this inhomogeneous leading-edge region which conflicts somewhat with the requirement that x_1/L_∞ should be no more than $O(1)$ for RDT to apply.

Perot & Moin (1995) analysed the plane wall case by direct simulation of the full Navier–Stokes equations. No RDT assumptions are therefore made and computations were carried out for turbulence Reynolds numbers $\kappa^2/\nu\epsilon$, κ being the turbulence energy and ϵ its dissipation rate, up to 374. In these numerical experiments the problem was transferred to the time domain in which an infinite plane wall was materialized at time $t = 0$ into a previously homogeneous field of turbulence and the subsequent time evolution studied. This type of realization removes the initial streamwise inhomogeneity along the wall owing to the leading edge. Perot & Moin examined three different boundary condition cases: (i) zero tangential velocity with consequently zero normal velocity gradient, (ii) zero normal velocity with zero tangential velocity gradient (zero shear) and (iii) zero normal and tangential velocity at the wall. The results for cases (ii) and (iii) for which the zero normal velocity boundary condition applies show that the result of RDT given in HG is correct in the limit $Re_T \to \infty$ for very small times after the boundary insertion. Subsequent evolution of the turbulent wall layer should be seen as evolution of the turbulence away from this initial RDT state as the neglected nonlinear and viscous terms take effect. In case (iii), the solid wall, the evolution of tangential Reynolds stress away from the initial RDT peak at the wall is very evident but the normal Reynolds stress in both cases (ii) and (iii) appears to continue to be damped at a rate close but not exactly equal to that predicted in HG. The results have been generally confirmed by the experiments of Aronson *et al*. (1997). A DNS analysis of turbulence suddenly brought into contact with a free surface, case (ii) studied by Perot & Moin, has also been carried out by Walker, Leighton & Garza-Rios (1996) who examined this case in great detail and obtained results in general agreement with those of Perot & Moin.

These studies have been motivated by practical problems such as those relating to the prediction of turbulent ship-wake signatures in the ocean as well as the desire to obtain a better understanding of the mechanisms controlling wall turbulence. Near-wall effects are of great importance in Reynolds average turbulence models for boundary layers. Wall damping functions (e.g. Gibson & Launder 1978) have been developed to simulate the effects, but up to the present still over-simplify the long-term evolution of turbulence adjacent to a wall.

The present paper is concerned with the rapid distortion of a convected turbulence field incident on and emerging from an infinite, unstaggered cascade of flat plates, with the assumption that any turbulence production from the boundary layers and wakes of the elements of the cascade is restricted to very thin regions and if necessary is sufficiently removed in scale to be separated out or ignored. The plates are therefore assumed to present an infinite stack of plane surfaces of finite streamwise extent (chord) which are nominally shear free and tend to suppress one transverse component of the turbulence. Dowling (1985), Balakumar & Widnall (1986) and Atassi & Gebert (1987) have all studied theoretically the related problem of the interaction of a large eddy break-up device (LEBU) with representations of incident turbulence in a boundary layer. Dowling (1985) carried out a two-dimensional analysis of the interaction of the LEBU in the form of a short plate above a wall with a single vortex representing an eddy. Balakumar & Widnall (1986) and Atassi & Gebert (1987) each analysed the effect of a short streamwise plate of infinite span placed above a plane wall on the individual three-dimensional Fourier components of the turbulence. The former followed an approach developed for the thin aerofoil/oblique gust problem (Reissner 1947; Graham 1970) approximating the solution to obtain results for the downstream flow field. The latter solved the problem numerically and similarly calculated the downstream velocity field. All these studies found the normal component of fluctuating

velocity downstream of the device to be considerably reduced, the most effective reduction being obtained for wavenumbers of the order of the inverse of the device chordlength. Also it appeared that the reduction obtained became less as the distance between the LEBU and the wall was reduced. In the present work we consider the case of a cascade of plates of long chord compared with the lengthscale of the turbulence. A much simpler expression can then be obtained for the downstream velocity field which allows the statistics of the resulting turbulence to be calculated without excessive computation.

When convected turbulence interacts with a shear free plane surface, RDT predicts that downstream of the ($O(L_\infty)$) leading-edge region the response or image field of the turbulence in the surface is homogeneous in the plane of the surface, convected with the free-stream turbulence at speed U_∞ and hence gives rise to a purely kinematic field with no induced pressure field. If the imposed boundary is a two-sided streamwise plate of sufficient length intersecting the turbulence, then the wall layers which occur on either side of this plate will be of similar form downstream of the leading-edge region. For a finite-length plate the turbulence leaving the downstream end does not immediately revert to homogeneity in the direction normal to the interface, even within the limits of RDT, because of the presence of a vortex wake shed from the trailing edge of the plate. This vorticity is associated with the changes in circulation around the plate and is additional to any viscous, momentum defect wake which may also be generated. In the limit of infinite Reynolds number and zero plate thickness, the vortex wake forms an infinitessimally thin sheet of vorticity of strength specified by the Kutta–Joukowski trailing-edge condition and convected at the free-stream speed. If the plate is long enough for the trailing edge to be clear of the leading-edge region so that a homogeneous region is formed on the plate, the wake sheet generates the same purely kinematic field as does the plate in the homogeneous region. The wake sheet therefore acts like a stress-free surface which continues the normal velocity damping effect of the plate. Its effect continues downstream of the trailing edge of the plate until long-term interaction with the turbulence field causes sufficient distortion of the wake vorticity to destroy its effect. The Kutta–Joukowski trailing-edge condition is the usual inviscid condition which specifies continuity of pressure across a sharp trailing edge of a plate or aerofoil. At finite Reynolds numbers and for non-zero trailing-edge thickness the Kutta–Joukowski condition may not be a very good approximation to the flow conditions for scales comparable with the wake displacement thickness at the trailing edge but is satisfactory for the larger scales.

In the case of a cascade, it is expected that the normal component of the turbulence will continue to be suppressed downstream as if the plates of the cascade extended much further. Within the framework of RDT this is a consequence of the vortex sheets. Figure 1 shows, as an example of this, a plot of the RMS streamwise and normal velocity components of grid generated turbulence after it has passed through a cascade of thin aerofoils. Also shown are the same components at the same downstream distances from the grid in the absence of the cascade. It is clear that the normal component of velocity is strongly suppressed and remains so while the streamwise component is less strongly affected. The main case evaluated theoretically is that when the cascade gap tends to zero on the lengthscale of the turbulence. This cascade has the strongest effect but for an inviscid analysis the Reynolds number must be high enough for the viscous layers to be negligible.

In practice, turbulence interacts with a cascade of aerofoils whenever it enters a blade row in a turbomachine. In these cases the incident turbulence either is present in the inlet flow to the engine owing to ingestion of atmospheric turbulence or wakes and

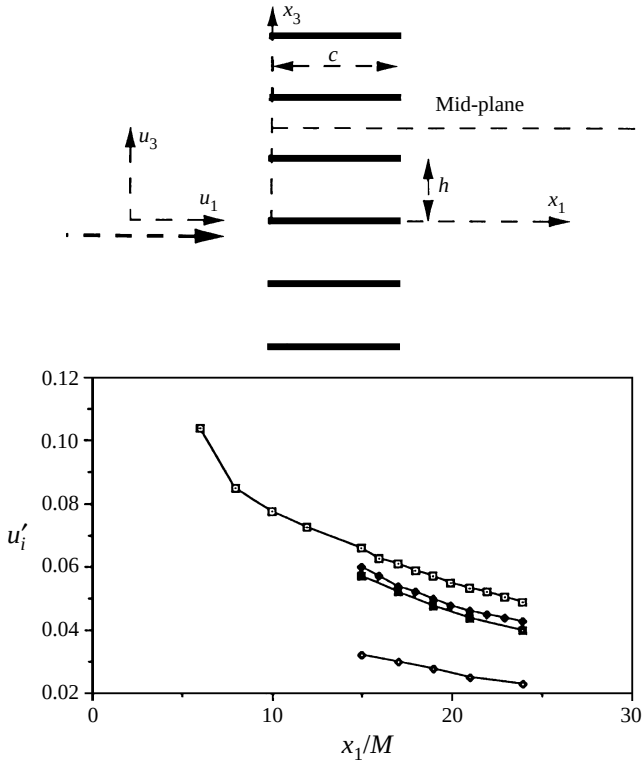

FIGURE 1. Measured r.m.s. turbulence velocities u_1 and u_3 with and without a cascade. Without cascade: □, $u_{1\infty}'$; ◆, $u_{3\infty}'$. With cascade: ■, $u_{1\infty}'$; ◇, $u_{3\infty}'$.

boundary layers originating upstream of the inlet or it arises from upstream components such as other blade rows in the machine. Many different scales may be present and the geometry is more complex than is considered here. Mean flow curvature is one of the significant effects on the turbulence (Maxey 1978) which is not considered in the present analysis. The main concern in turbomachinery is with induced effects of loading, noise and heat transfer. In another field, honeycombs and other flow straighteners in wind tunnels and ducts interact with free-stream turbulence and are used as turbulence suppressors. They affect the flow by a combination of streamwise viscous resistence and transverse velocity suppression.

Interaction of homogeneous free-stream turbulence with linear cascades of thin aerofoils at zero or small mean incidence has been analysed for general cases by Kullar & Graham (1986). The main aim of that work was to predict the loadings induced on the cascade and in compressible cases the associated acoustic pressure field using analysis based on unsteady thin aerofoil theory. The assumption was made that the flow conditions were such that the cascade generated a linear response to the turbulence which could be calculated for individual wavenumbers independently of any mean strain field and the results superposed. This approach is equivalent to the HG analysis and makes the same assumptions. In the case of a cascade of high solidity (small h) the leading-edge effect is shown to be confined to a region behind the leading edge of length of order h, the cascade spacing. It is therefore more possible if the spacing is small to obtain a region within and downstream of the cascade where the flow field can be treated as homogeneous in the streamwise direction but is still close

enough to the onset of the disturbance to the incident turbulent flow for the RDT assumptions to hold.

2. Theory

The flow geometry, as shown in figure 1, consists of a linear, unstaggered cascade of thin plates

$$0 < x_1 < c, \quad -\infty < x_2 < \infty, \quad x_3 = nh, \quad -\infty < n < \infty,$$

at zero incidence through which an incompressible, turbulent flow passes at mean speed U_∞. For the purposes of this analysis the origin of coordinates is located at the leading edge of one of the plates with x_1 streamwise, x_2 spanwise and x_3 normal. For some later comparisons with measured data the origin of x_1 is shifted forward to the turbulence grid.

The incident turbulence has corresponding velocity components $(u_{1\infty}, u_{2\infty}, u_{3\infty})$ and is characterized by its longitudinal integral lengthscale L_∞. We consider first the case:

$$h \ll L_\infty. \tag{1}$$

The chord c of the plates is assumed to be of order L_∞. This cascade for which the relative spacing tends to zero in the limit is one which will have the strongest effect on suppressing the normal velocity component of the turbulence as it passes through. It is assumed that the Reynolds number of the flow is sufficiently high for an inviscid analysis to be appropriate. Hence, the plates act to block the normal component of the turbulence u_3 but steady and unsteady viscous boundary layers and wakes are thin enough to be neglected. In the notation of HG, $B^{(v)} \to 0$ and we concentrate on the source layer $B^{(s)}$ which arises owing to the blocking action.

Since the mean flow U_∞ is undisturbed by the cascade and since quadratic and viscous terms are neglected (RDT), the transport equation for the vorticity ζ of the turbulence is:

$$\partial\zeta/\partial t + U_\infty \, \partial\zeta/\partial x_1 = 0. \tag{2}$$

The whole vorticity field is convected with the free-stream speed U_∞ as a frozen distribution and the effect of the plate on the turbulence is irrotational outside the wake.

The incident turbulence velocity field is assumed to be homogeneous and can therefore be represented by the Fourier integrals:

$$\boldsymbol{u}_\infty(\boldsymbol{x}, t) = \iiint \hat{\boldsymbol{u}}_\infty(\boldsymbol{k}) \exp \mathrm{i}(\omega t - k_j x_j) \, \mathrm{d}\boldsymbol{k}, \tag{3}$$

with $\omega = k_1 U_\infty$ from equation (2).

Provided the chord c of the plates is sufficiently large, there exists a region of streamwise homogeneity on the plates where the direct influence of the leading edge has become negligible. In the case of an isolated plate with $c \gg L_\infty$ the region of influence of the leading edge was shown in HG (Appendix A) to extend a distance of about L_∞ downstream of the leading edge. Since RDT really only applies within a distance of about L_∞ from the leading edge (Perot & Moin 1995; Aronson *et al.* 1997) the extent over which both RDT and planewise homogeneity may be simultaneously assumed to apply accurately is very limited. However, the RDT prediction of the component of Reynolds stress normal to the plate agrees reasonably well with measurements over a much longer distance (Thomas & Hancock 1977). In the case of a cascade with small spacing $h \ll L_\infty$, the inhomogeneous leading-edge region is smaller, only extending a distance $O(h)$. The flow within a cascade having $c = O(L_\infty)$ will therefore be homogeneous within a longer region. The flow field is also homogeneous in the

spanwise direction and therefore each Fourier component of the flow field can be expressed as:

$$\boldsymbol{u}(\boldsymbol{k}) = \hat{\boldsymbol{u}}_\infty(\boldsymbol{k}) \exp \mathrm{i}(\omega t - k_j x_j) + \boldsymbol{\nabla}\{\hat{\phi}(\boldsymbol{k}, x_3) \exp \mathrm{i}(\omega t - k_1 x_1 - k_2 x_2)\}, \tag{4}$$

where ϕ is the velocity potential due to the blocking effect of the cascade. Since the velocity field is divergence-free, $\hat{\phi}$ satisfies:

$$\partial^2 \hat{\phi}/x_3^2 - (k_1^2 + k_2^2)\,\hat{\phi} = 0, \tag{5}$$

with the boundary condition on the plate:

$$\frac{\partial \hat{\phi}}{\partial x_3} + \hat{u}_{3\infty} \exp(-\mathrm{i} k_3 nh) = 0 \quad \text{on} \quad x_3 = nh, \quad n = \text{all } \pm \text{ integers}. \tag{6}$$

The solution to (5) and (6) for the flow field in the region between plates n and $n+1$ is:

$$\hat{\phi} = \frac{-\hat{u}_{3\infty}}{\tau} f(k_3, \tau, x_3') \exp(-\mathrm{i} k_3 nh), \tag{7}$$

where

$$\tau = (k_1^2 + k_2^2)^{1/2},$$

$$f(k_3, \tau, x_3') = \frac{\{\cosh(\tau x_3') \exp(-\mathrm{i} k_3 h) - \cosh(\tau[h - x_3'])\}}{\sinh(\tau h)}$$

and x_3' is the local coordinate: $0 \leqslant x_3' (= x_3 - nh) \leqslant h$.

Hence

$$u_1 = \left(\hat{u}_{1\infty} \exp(-\mathrm{i} k_3 x_3') + \frac{\mathrm{i} k_1}{\tau} \hat{u}_{3\infty} f(k_3, \tau, x_3')\right) \exp(\mathrm{i}(\omega t - k_1 x_1 - k_2 x_2 - k_3 nh)), \tag{8}$$

$$u_2 = \left\{\hat{u}_{2\infty} \exp(-\mathrm{i} k_3 x_3') + \frac{\mathrm{i} k_2}{\tau} \hat{u}_{3\infty} f(k_3, \tau, x_3')\right\} \exp(\mathrm{i}(\omega t - k_1 x_1 - k_2 x_2 - k_3 nh)), \tag{9}$$

and

$$u_3 = \hat{u}_{3\infty} \left(\exp(-\mathrm{i} k_3 x_3') - \frac{\sinh(\tau x_3') \exp(-\mathrm{i} k_3 h) + \sinh(\tau[h - x_3'])}{\sinh(\tau h)}\right) \exp(\mathrm{i}(\omega t - k_1 x_1 - k_2 x_2 - k_3 nh)). \tag{10}$$

At the trailing edge of each plate, owing to the change in the circulation generated around the plate a vortex sheet is shed into the wake. In this linear approximation, consistent with RDT, the vortex sheet shed from each plate is assumed to be coplanar with the plate, in $c \leqslant x_1 < \infty$, $-\infty \leqslant x_2 < \infty$ and $x_3 = nh$.

Assuming the Kutta–Joukowski condition of zero pressure difference at the trailing edge, the jump in potential across the sheet, $\Delta\phi_{(\mathrm{wake})}$, satisfies:

$$\Delta\phi_{(\mathrm{wake})} = \phi|_{x_3 = nh+} - \phi|_{x_3 = nh-} \tag{11}$$

at the trailing edge $x_1 = c$ on the two sides, $x_3 = nh\pm$, of the nth plate.

To the same order, continuity of pressure across the vortex sheet implies that:

$$(\partial/\partial t + U_\infty \partial/\partial x_1)\,\Delta\hat{\phi}_{(\mathrm{wake})} = 0. \tag{12}$$

Conditions (11) and (12) lead to the solution for the potential associated with the wake sheet:

$$\hat{\phi} = \frac{-\hat{u}_{3\infty}}{\tau} f(k_3, \tau, x_3') \exp(-\mathrm{i} k_3 nh) \quad (c \leqslant x_1 < \infty). \tag{13}$$

The wake potential field (13) and hence the velocity field between the wake sheets is the same as that given by (7)–(10) for the flow field within the cascade, both fields being

convected at the free-stream speed. This is consistent with the fact that since to this order there is no disturbance pressure field induced by the turbulence on any plate of the cascade downstream of the leading-edge region, there is no pressure discontinuity across the plate just as there is no pressure jump across its wake sheet. The loading induced by the turbulence is concentrated in the leading-edge region of each plate, Kullar & Graham (1986). Downstream of the leading-edge region the effects of a streamwise plate and its wake are therefore indistinguishable according to the assumptions of RDT. The wake sheet may also be considered to be the vorticity shed by the plate owing to its varying circulation or in the limit of infinite Reynolds number the result of shedding the plate surface vortex sheets which accommodate a no-slip condition beneath the potential flow.

This result which applies to all streamwise plates whose chords extend beyond the leading-edge region, is central to the prediction of the suppression by a cascade of the normal velocity component of turbulence emerging on its downstream side. It is therefore also worth comparing the distributions of measured and predicted normal velocity component downstream of a single (isolated) streamwise plate for which the same conditions apply. In that case the above analysis predicts that for a long enough plate, $c \gg L_\infty$ on $x_3 = 0$ the turbulent velocity field induced in the wake region $x_1 > c$, $O(-L_\infty) < x_3 < O(L_\infty)$ is the same as that given in HG for the $B^{(s)}$ field above a plane wall. Although RDT should strictly be limited to $x_1 \sim L_\infty$ the results for the u_3 field are predicted well for a much longer streamwise extent. It might therefore be expected that measurements of $\overline{u_3^2}$ downstream of the plate would also be in reasonable agreement with the theoretical prediction whereas $\overline{u_1^2}$ and $\overline{u_2^2}$ would have evolved away from the RDT prediction. The true boundary condition at $x_3 = 0$, $x_1 > c$, now matches the velocities and stresses across an interface in the wake following the initial no-slip region on the plate.

An intermediate result which is also evaluated in the present paper is that for the flow behind a (biplane) pair of plates which, if of long enough chord, should exhibit the same flow field as an infinite cascade in the gap between the wakes of the two plates and the same flow field as the isolated plate in the regions outside the wake pair. These two results will be considered in more detail later.

In the case of the infinite cascade, although not physically realizable except approximately, it is of interest to calculate the effect of the obstruction on the turbulence in the limit of very high solidity when the ratio of the cascade spacing h to the turbulence lengthscale L_∞ tends to zero. This is the case for which the cascade has the strongest effect on the turbulence and for which the theoretical results are simplest.

Taking the limit $h/L_\infty \to 0$ with Re_T large enough ($\gg (x_1/L_\infty)(h/L_\infty)^{-2}$) that the viscous layers remain much thinner than the gap h, and hence with $k_j h \to 0$ in equations (8)–(10) gives:

Therefore:

$$f(k_3, \tau, x_3') \to -\mathrm{i}k_3/\tau, \quad k_3 nh \to k_3 x_3.$$

$$u_1 \to \left(\hat{u}_{1\infty} + \frac{k_1 k_3}{\tau^2}\hat{u}_{3\infty}\right)\exp(\mathrm{i}(\omega t - k_j x_j)), \tag{14}$$

$$u_2 \to \left(\hat{u}_{2\infty} + \frac{k_2 k_3}{\tau^2}\hat{u}_{3\infty}\right)\exp(\mathrm{i}(\omega t - k_j x_j)), \tag{15}$$

$$u_3 \to 0. \tag{16}$$

The three-dimensional spectrum function Φ_{ij} describing the turbulence is formed from the products of the Fourier amplitudes $\hat{u}_j$, see e.g. HG. Thus $\Phi_{ij} = \hat{u}_i \hat{u}_j^*$, where * indicates a complex conjugate. From here on, for convenience, all wavenumbers and lengths are assumed to be non-dimensionalized by L_∞.

Therefore, the turbulence spectrum function Φ_{ij} downstream of a cascade which suppresses u_3, is related to $\Phi_{ij\infty}$ for the incident upstream turbulence by

$$\Phi_{ij} = \Phi_{ij\infty} + \frac{k_3}{\tau^2}(k_j \Phi_{i3\infty} + k_i \Phi_{3j\infty}) + \frac{k_i k_j k_3^2}{\tau^4}\Phi_{33\infty} \quad (i,j \neq 3). \tag{17}$$

If we now assume that the upstream turbulence is isotropic:

$$\Phi_{ij\infty} = \left(\delta_{ij} - \frac{k_i k_j}{k^2}\right) E_\infty(k^2), \tag{18}$$

where δ_{ij} is the Kronecker delta and $E_\infty(k^2)$ is the energy density of the incident turbulence at wavenumber $\boldsymbol{k}$.

Hence downstream:

$$\begin{aligned}\Phi_{ij} &= \left(\delta_{ij} - \frac{k_i k_j}{\tau^2}\right) E_\infty(k^2) \quad (i,j \neq 3) \\ &= 0 \quad \text{if } i \text{ or } j = 3.\end{aligned} \tag{19}$$

This turbulence is isotropic in the $(1,2)$ plane normal to the axis of the cascade. Integration of (19), over all wavenumbers:

$$\overline{u_1^2} + \overline{u_2^2} = \iiint (\Phi_{11} + \Phi_{22})\,\mathrm{d}k = \iiint E_\infty(k^2)\,\mathrm{d}k = \tfrac{1}{2}(\overline{u_{1\infty}^2} + \overline{u_{2\infty}^2} + \overline{u_{3\infty}^2}), \tag{20}$$

showing that the total energy has been reduced by a half.

Since the velocity variances for isotropic turbulence are equal:

$$\overline{u_1^2} = \overline{u_2^2} = \tfrac{3}{4}\overline{u_{1\infty}^2} \quad \overline{u_3^2} = 0. \tag{21}$$

Thus $\overline{u_1^2}/\overline{u_{1\infty}^2}$ and $\overline{u_2^2}/\overline{u_{2\infty}^2}$ are predicted by RDT to be reduced by a cascade in contrast to the predicted increase of both these Reynolds stress ratios to a value of 1.5 at the surface of an isolated plate. The results may also be contrasted with a previous analysis of the effect of a dense cascade (Basuki 1983) as a 'refracting' surface like a gauze. This analysis followed the approach of Batchelor & Proudman (1954) in analysing the effect of a gauze on homogeneous, isotropic turbulence. The effect of the cascade was assumed to be represented by a refraction coefficient α operating only on the u_3 component of the velocity field, leading in the limit of high solidity, $\alpha \to 0$, to:

$$\Phi_{ij} = \Phi_{ij\infty} + F_j \Phi_{i3\infty} + F_i \Phi_{3j\infty} + F_i F_j \Phi_{33\infty} \quad (i,j = 1,2,3), \tag{22}$$

with $$F_1 = 2k_1 k_3 f', \quad F_2 = 2k_2 k_3 f', \quad F_3 = k_3^2\left(1 - \frac{\mathrm{i}k_1}{(k_2^2 + k_3^2)^{1/2}}\right) f',$$

and $$f' = 2k^2 - k_3^2 - \frac{\mathrm{i}k_1 k_3^2}{(k_2^2 + k_3^2)^{1/2}}.$$

From this refraction analysis the predicted downstream turbulence is not isotropic in the $(1,2)$ plane and the u_3 component is never completely suppressed.

3. Frequency spectra and lengthscales

The one-dimensional (frequency) spectrum is defined as:

$$\Theta_{ii}(k_1) = \iint_{-\infty}^{\infty} \Phi_{ii}(\boldsymbol{k})\,\mathrm{d}k_2\,\mathrm{d}k_3. \tag{23}$$

Applying this to equation (19) leads to:

$$\Theta_{11}(k_1)+\Theta_{22}(k_1)=\iint_{-\infty}^{\infty}E_\infty(\boldsymbol{k})\,\mathrm{d}k_2\,\mathrm{d}k_3=\tfrac{1}{2}\{\Theta_{11\infty}(k_1)+\Theta_{22\infty}(k_1)+\Theta_{33\infty}(k_1)\} \quad (24)$$

with $$\Theta_{33}(k_1)=0.$$

Since $$\Theta_{22}(k_1)=\iint_{-\infty}^{\infty}\frac{k_1^2}{\tau^2}E_\infty(k)\,\mathrm{d}k_2\,\mathrm{d}k_3 \quad \text{and} \quad \int_{-\infty}^{\infty}E_\infty(k_2^2+k_3^2)\,\mathrm{d}k_3$$

is finite,

$$\Theta_{22}(k_1)=O(k_1) \quad \text{as} \quad k_1\to 0.$$

Hence for isotropic turbulence for which $\Theta_{11\infty}(0)=2\Theta_{22\infty}(0)=2\Theta_{33\infty}(0)$,

$$\Theta_{11}(k_1)\to\Theta_{11\infty}(0) \quad \text{as} \quad k_1\to 0.$$

Correspondingly for the dimensional lengthscales:

$$\begin{aligned}
&L_{11x1}\equiv\int_0^{\infty}\overline{u_1\,u_1}(x_1')\,\mathrm{d}x_1'=L_\infty,\\
&L_{22x1}=0,\\
&L_{22x2}=L_\infty,\\
&L_{11x2}=0,\\
&L_{11x3}=(\overline{u_{1\infty}^2}/\overline{u_1^2})\,L_{11x3\infty}=\tfrac{4}{3}L_{11x2\infty}=\tfrac{2}{3}L_\infty
\end{aligned}$$

and

$$L_{22x3}=\tfrac{2}{3}L_\infty.$$

In order to compute spectra it is necessary to assume a distribution for the incident energy spectrum $E_\infty(k^2)$. A commonly used form for isotropic turbulence is the Von Kármán spectrum:

$$E_\infty(k^2)=\frac{g_3\,k^2}{(g_2+k^2)^{17/6}}, \quad (25)$$

where $g_2=0.558$ and $g_3=0.09507$. This gives the one-dimensional frequency spectrum:

$$\Theta_{11\infty}=\frac{g_1}{(g_2+k_1^2)^{5/6}}, \quad \text{where} \quad g_1=0.1955. \quad (26)$$

Therefore the one-dimensional spectrum of streamwise velocity downstream of the cascade:

$$\begin{aligned}
\Theta_{11}(k_1)&=g_3\iint_{-\infty}^{\infty}\left(k_2^2+k_3^2-\frac{k_1^2k_3^2}{(k_1^2+k_2^2)}\right)\frac{\mathrm{d}k_2\,\mathrm{d}k_3}{(g_2+k^2)^{17/6}}\\
&=\Theta_{11\infty}(k_1)-\frac{g_4}{k_1^{5/3}}I\left(1+\frac{g_2}{k_1^2}\right)\\
&=\frac{g_1}{(g_2+k_1^2)^{5/6}}-\frac{g_4}{k_1^{5/3}}I\left(1+\frac{g_2}{k_1^2}\right), \quad (27)
\end{aligned}$$

where

$$I(a)=\int_0^{\infty}\frac{\mathrm{d}\lambda}{(1+\lambda^2)\,(a+\lambda^2)^{4/3}}, \quad g_4=0.08726.$$

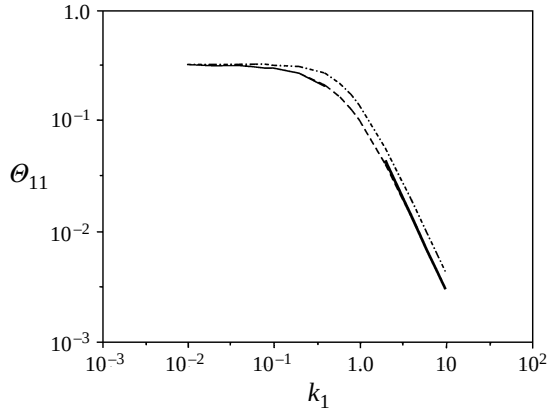

FIGURE 2. Turbulence spectrum Θ_{11} predicted by RDT. –·–, $\Theta_{11\infty}$; – – –, Θ_{11}; ——, asymptotes.

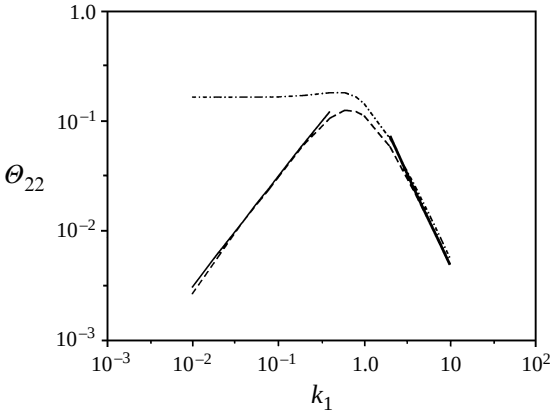

FIGURE 3. Turbulence spectrum Θ_{22} predicted by RDT. –·–, $\Theta_{22\infty}$; – – –, Θ_{22}; ——, asymptotes.

Similarly:

$$\Theta_{22}(k_1) = \tfrac{1}{2}(\Theta_{22\infty}(k_1)+\Theta_{33\infty}(k_1)-\Theta_{11\infty}(k_2))+\frac{g_4}{k_1^{5/3}}I\left(1+\frac{g_2}{k_1^2}\right)$$
$$= \frac{5}{6}\frac{g_1 k_1^2}{(g_2+k_1^2)^{11/6}}+\frac{g_4}{k_1^{5/3}}I\left(1+\frac{g_2}{k_1^2}\right). \tag{28}$$

The asymptotic behaviour of the integral I is:

$$I(k_1\to 0) \sim \pi/2\, g_2^{-4/3}k_1^{8/3},$$
$$I(k_1\to \infty) \sim 1/2\Gamma(1/2)\,\Gamma(11/6)/\Gamma(7/3).$$

Hence the asymptotic behaviour of the turbulence spectra downstream of the cascade is:

$$k_1\to 0, \quad \Theta_{11} \sim 1/\pi - 0.298k_1,$$
$$\Theta_{22} \sim 0.298k_1$$

and

$$k_1\to \infty, \quad \Theta_{11} \sim g_5 k_1^{-5/3}, \quad g_5 = 0.1344,$$
$$\Theta_{22} \sim 5/3 g_5 k_1^{-5/3}.$$

The main ranges of Θ_{11} and Θ_{22} are plotted in figures 2 and 3. The crossover point,

$k_1 \approx 0.9$, for the two spectra is approximately unchanged by the cascade and as already stated the downstream intensities $\overline{u_1^2}$ and $\overline{u_2^2}$ are predicted to remain equal. However, the ratio of the PSDs at the high frequency end of the two spectra $\Theta_{11}:\Theta_{22}$ changes from 3/4 upstream of the cascade to 3/5 downstream. Similarly, consistent with the fact that $L_{22x1} = 0$, the low-frequency components of the non-damped transverse velocity fluctuations, u_2, are greatly reduced.

4. Comparisons with measured results for grid generated turbulence

Comparisons of the above results can be carried out with nearly homogeneous isotropic turbulence generated by a grid in a wind tunnel, then passed through a linear cascade of thin aerofoils or flat plates. The finite gap h between the elements of the cascade reduces their effect on the turbulence. The maximum effect is then predicted to occur on each of the planes of the cascade, $x_3 = nh$, coplanar with the elements and the minimum effect on the planes $x_3 = (n+\frac{1}{2})h$, midway between. For sufficiently large aerofoil chords the normal component u_3 is still predicted to be reduced to zero on the $x_3 = nh$ planes. In practice, the measured value of this component will be larger than zero because of production in the aerofoil boundary layers and wakes and break-up of the vortex sheet. Also, as discussed earlier, the assumptions of rapid distortion theory are less tenable with increasing downstream distance from the point of onset of the distortion. The value of the turbulence on the midplane of the gaps, $x_3 = (n+\frac{1}{2})h$, should be less affected by some of these effects and may be calculated by extending the analysis to the case of finite gaps.

5. Turbulence downstream of a single plate

As a first test, measurements were made of the $\overline{u_1^2}$ and $\overline{u_3^2}$ components of the Reynolds stress just downstream of the trailing edge of a single thin streamwise plate, equivalent to removing all but one plate of the cascade which is retained in isolation in the mid-plane of the wind tunnel in a turbulent flow. A biplanar grid with mesh of side $M = 150$ mm and rectangular section bars of width 25 mm was used to generate the turbulence. Turbulent flows past two different plates spanning the working section of the tunnel were measured. Both plates had a thickness of 2 mm with rounded leading and chamfered trailing edges. One plate had a chord $c = 250$ mm and the other $c = 125$ mm and each was placed in the tunnel with its leading edge at a distance of $10M$ downstream of the grid. Measurements were carried out using hot-wire anemometry at one mean flow speed giving a Reynolds number at the leading edge based on the grid mesh of approximately 3×10^5 and a turbulence Reynolds number ($u'_\infty L_\infty/\nu$) of about 10^4 (or $\kappa^2/\nu\epsilon$ of about 5×10^3). The ratio L_∞/c was 0.20 and 0.41, respectively, for the two plates. The rounded leading edges of the plates in these experiments were made small as a compromise between sharp leading edges with the attendant problem of leading-edge separation owing to the incidence changes in the incident turbulent flow and edges with considerable rounding similar to aerofoil leading edges used in the other cascade experiments. All leading edges generate a region of large mean strain around the stagnation line with attendant complex distortion of turbulence passing through. The larger the rounding the more extensive is this region of distortion.

For single, isolated plates the wake is predicted to act as a stress free surface continuing the normal velocity damping effect of the plate. The variation in Reynolds stresses predicted by RDT for the region of the plate plane are as given in HG (figure 5), but now on both sides of $x_3 = 0$. These theoretical predictions and the measured

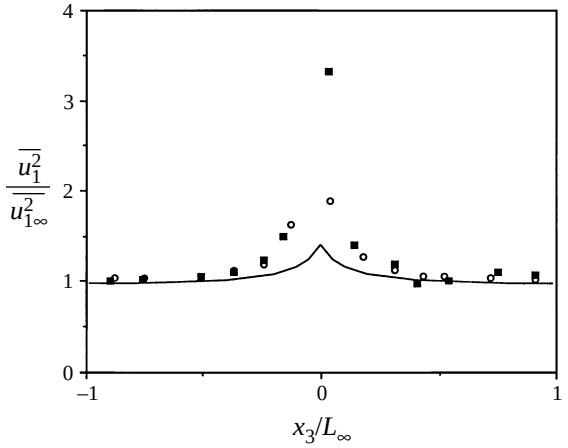

FIGURE 4. $\overline{u_1^2}/\overline{u_{1\infty}^2}$ measured downstream of a single plate. ○, $x_1/M = 12.1$; ■, $x_1/M = 13.1$; ——, RDT theory.

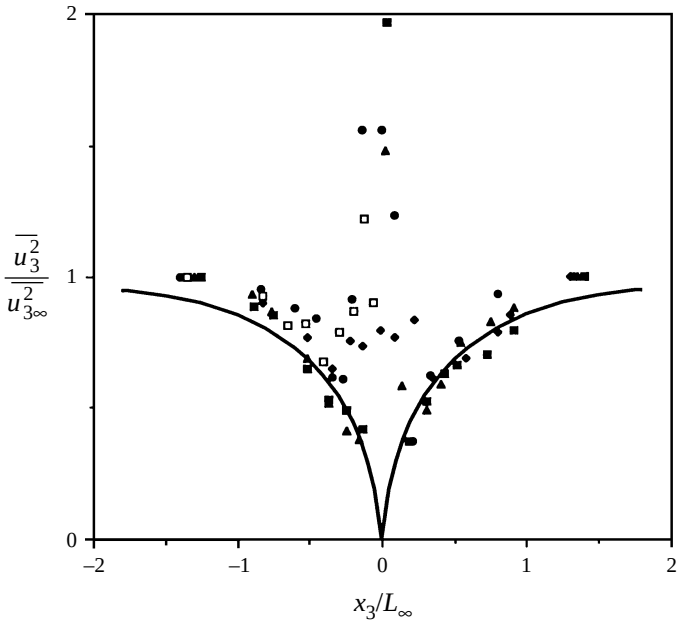

FIGURE 5. $\overline{u_3^2}/\overline{u_{3\infty}^2}$ measured downstream of a single plate. Long plate: □, $x_1/M = 11.6$; ●, $x_1/M = 12.1$; ◆, $x_1/M = 13.1$. Short plate: ▲, $x_1/M = 12.1$; ■, $x_1/M = 13.1$; ——, RDT theory.

results for $\overline{u_1^2}$ and $\overline{u_3^2}$ taken at different stations downstream of the trailing edges of each of the plates, and in one case just upstream (i.e. adjacent to the plate surface rather than its wake) for comparison, are shown in figures 4 and 5. Here and throughout the following comparisons the Reynolds stresses are shown divided by the corresponding free-stream value at the same x_1 station in order to attempt to remove the main effects of streamwise decay. Both components of Reynolds stress show significant increases in the region close to $x_3 = 0$. This is mainly due to the mean shear in the boundary layer and wake regions of the plates giving rise to additional turbulence production but may

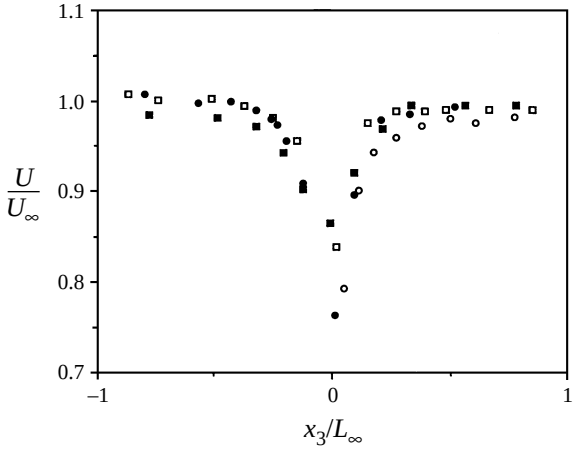

FIGURE 6. $U(x_3)/U_\infty$ measured downstream of a single plate. Long plate: ○, $x_1/M = 12.1$; ■, $x_1/M = 13.1$. Short plate: □, $x_1/M = 12.1$; ●, $x_1/M = 13.1$.

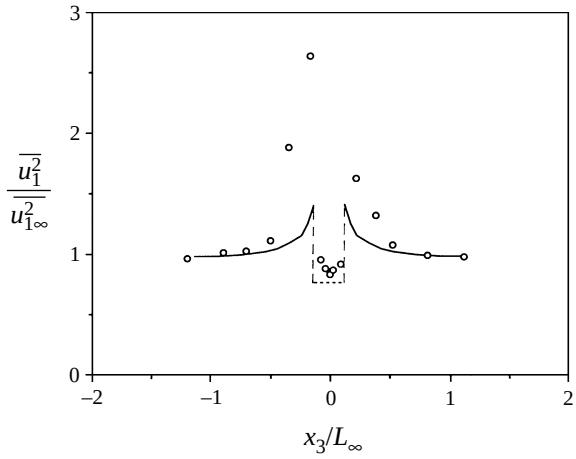

FIGURE 7. $\overline{u_1^2}/\overline{u_{1\infty}^2}$ measured downstream of a double plate. ○, $x_1/M = 11.3$; ——, RDT theory (single surface); – – –, RDT theory (cascade, $h/L_\infty = 0$).

also include some of the effects of RDT failure to predict streamwise evolution of the turbulence as x_1/L_∞ becomes large. Figure 6 shows the wake regions of the mean velocity corresponding quite well to the regions of raised Reynolds stress, the shorter plate generating a slightly thinner region. Outside these regions $\overline{u_3^2}$ shows the damping of the normal velocity component to be in fair agreement with the theoretical curve. $\overline{u_1^2}$ shows a tendency to increase outside the region where production due to mean shear is significant, which is also in apparent agreement with the theory. In HG the theoretical predictions were compared with measurements taken by Thomas & Hancock (1977) in the turbulent wall layer, nominally without mean shear, above a moving wall. These comparisons showed the measured $\overline{u_1^2}$ data to lie above the predicted curve by an increasing amount and with a large peak near the wall as the turbulence is convected downstream. Perot & Moin (1995) have discussed this result and shown it to be due, at least partly, to reduced dissipation near the wall relative to the dissipation in the free stream, bearing in mind that the Reynolds stresses are all

non-dimensionalized on their corresponding free-stream values at the same streamwise station. The measurements of Aronson *et al.* (1997) made at lower Reynolds numbers than those of Thomas & Hancock, closer to the values used in the computations of Perot & Moin, are in much better agreement with the latter. Aronson *et al.* showed, by applying an artificially raised wall temperature, that the raised $\overline{u_1^2}$ values could also have been partly due to contamination of the hot-wire velocity measurements by temperature fluctuations. Thomas & Hancock's experiment involved the use of a non-cooled moving wall from which some heating effect due to friction may have occurred. In the present case the measured data does also tend to lie above the theoretical curve. The same non-dimensionalization on local free-stream values has been used. There is no source of heating but there is a significant effect from the region of increased production by the mean shear adjacent to the plate and in its wake. There is no clear difference between the results for the different stations and plates beyond the effect of the different widths of these mean shear/production regions.

In the case of the Reynolds stress $\overline{u_3^2}$, as discussed by Walker *et al.* (1996), the dissipation of this component relative to its value near a (free) surface is high reducing the effect of pressure strain redistribution from the larger $\overline{u_1^2}$ to the smaller $\overline{u_3^2}$ near the surface, thus keeping the latter small in that region.

The present analysis also ignores the effects of distortion of the incident turbulence by the leading-edge stagnation zones of the cascade plates. Vorticity normal to the plates is wrapped around the leading edges, subject to intense local stretching balanced ultimately by viscous effects. This gives rise to additional streamwise vorticity and may explain greater than predicted velocity fluctuations in the normal and spanwise directions (Saxena 1994).

6. Turbulence downstream of a double plate

A second series of tests were carried out using a combination of two plates in a biplane arrangement, one above the other. In this case because the plate wake combinations are effectively semi-infinite the regions outside the wake pair should behave as for the single plate according to the above theory. The region between the wakes should be the same as if the pair of plates were part of an infinite linear cascade.

Reynolds stresses were measured just downstream of the double plate arrangement, at approximately the same Reynolds numbers as for the single plate, each plate of the pair having the same geometry as the shorter single plate described above. The plates were separated by a gap of 12.5 mm and placed in the same flow conditions as the single plates, so that $h/L_\infty = 0.25$ and $L_\infty/c = 0.41$. The measured results are compared with the theoretical predictions in figure 7 ($\overline{u_1^2}$) and figure 8 ($\overline{u_3^2}$). Outside the double wake the results are seen to be very similar to the single plate–single wake case. Between the wakes the measured results for $\overline{u_1^2}$ are compared with the predicted value $\overline{u_1^2}/\overline{u_{1\infty}^2} = 0.75$, for a cascade of infinitessimal gap (equation (21)). The predicted value of $\overline{u_3^2}$ which tends to zero for an infinitessimal gap is very sensitive to gap size and therefore the values predicted by equation (10) for a cascade with the appropriate non-zero gap are shown. The low-frequency ends of the predicted velocity spectra are similarly sensitive. These are discussed further in the next section for the infinite cascade with finite gap.

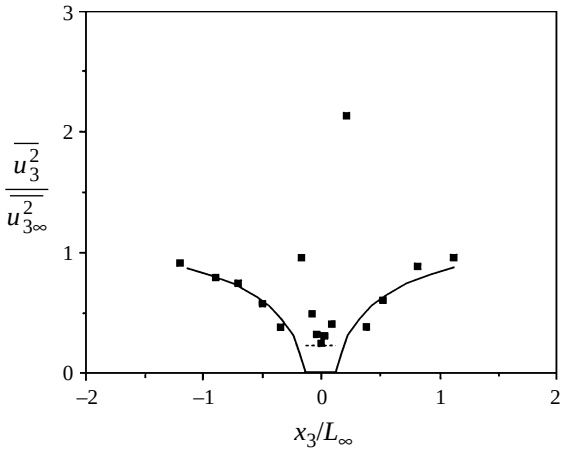

FIGURE 8. $\overline{u_3^2}/\overline{u_{3\infty}^2}$ measured downstream of a double plate. ■, $x_1/M = 11.3$; ——, RDT theory (single surface); – – –, RDT theory (cascade, $h/L_\infty = 0.25$).

7. Turbulence downstream of a cascade with finite gap

Experimental realizations of turbulence passing through cascades of plates or aerofoils inevitably involve a finite gap. The result for the suppressed component, u_3, of the turbulence is most strongly affected by the width of the cascade gap. Since this is also the component for which the measured results at large x_1 agree best with RDT it is appropriate to make the comparisons with theoretical predictions for finite gap width.

Measurements were taken downstream of various cascades of thin aerofoils covering a cross-section of a wind tunnel from floor to roof. The measurements were made at points either coplanar with an element (aerofoil) of the cascade or in a mid-plane halfway between two elements. In the former case RDT predicts $u_3 = 0$ for all gap widths, but the strong effects of production owing to the mean shear in these regions obscure this. The mid-plane results are therefore likely to offer a better comparison with the theory.

From equation (10) which, as was shown, applies equally to the downstream regions as to the gap between the aerofoils:

$$u_3(x_3 = (n+\tfrac{1}{2})\,h) = \hat{u}_{3\infty}\left(\exp(-\tfrac{1}{2}\mathrm{i}k_3 h) - \sinh(\tfrac{1}{2}\tau h)\frac{(1+\exp(-\mathrm{i}k_3 h))}{\sinh(\tau h)}\right). \tag{29}$$

Using the form of energy spectrum given in equation (25):

$$\begin{aligned} u_3(x_3 = (n+\tfrac{1}{2})\,h) &= g_3 \iiint_{-\infty}^{\infty} \left(1 - \frac{\cos(\tfrac{1}{2}k_3 h)}{\cosh(\tfrac{1}{2}\tau h)}\right)^2 \frac{\tau^2\,\mathrm{d}k}{(g_2 + k^2)^{17/6}} \\ &= (4h)^{2/3}\,\pi g_3 \iint_0^{\infty} \left(1 - \frac{\cos(\lambda)}{\cosh(\mu)}\right)^2 \frac{\mu^3\,\mathrm{d}\lambda\,\mathrm{d}\mu}{(\tfrac{1}{4}g_2 h^2 + \lambda^2 + \mu^2)^{17/6}}. \end{aligned} \tag{30}$$

Figure 9 shows the variation of the predicted downstream value of $\overline{u_3^2}$ on a mid-plane as a function of non-dimensional gap size (h/L_∞) as given by equation (30). According to the theory this should be the largest value of u_3^2 downstream of the cascade. For small gaps the limit of equation (30) as $h \to 0$ shows that $\overline{u_3^2}/\overline{u_{3\infty}^2} \sim 0.531(h/L_\infty)^{2/3}$. A value of $\overline{u_3^2}/\overline{u_{3\infty}^2} = 0.215$ is predicted for the mid-plane value downstream in the case of

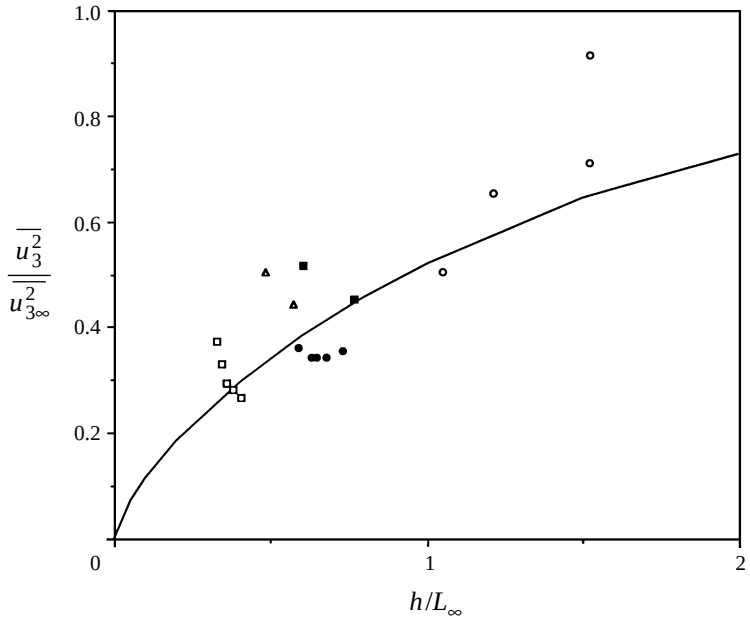

FIGURE 9. $\overline{u_3^2}/\overline{u_{3\infty}^2}$ on the centreplane behind a cascade versus gap size. ○, $M = 75$ mm; ●, ■, □, (different experiments) $M = 150$ mm; △, $M = 225$ mm.

the double plate shown in figure 8 which agrees quite well with the measured value. Because of the initial rapid increase in $\overline{u_3^2}$ with h, very small gaps with therefore greater viscous effects would be needed in practice to obtain nearly complete suppression of $\overline{u_3^2}$.

The wind-tunnel tests were carried out using linear, unstaggered cascades of aerofoils. The first cascade consisted of 20 aerofoils of NACA 0015 section and chord 79 mm spaced over the working section's 900 mm height at 45 mm spacing. The second consisted of 35 aerofoils of NACA 0008 section, 100 mm chord and 25 mm spacing. Turbulence was generated by a biplanar grid of the same mesh size of 150 mm as before but with a bar size of 38 mm. For the main tests the cascades were each placed at $11M$ downstream of the grid at which point the ratio L_∞/M was 0.38 and hence the ratio h/L_∞ took the values 0.79 and 0.44, respectively, for the two cascades. The turbulence Reynolds numbers were similar to those for the single plate tests. Further tests were also conducted with the first cascade at $23M$ downstream of the 150 mm grid. In this case $L_\infty/M = 0.50$ and the ratio $h/L_\infty = 0.6$. More details of these tests are given in Basuki (1983) and Haidos (1983). Results were also taken using a smaller 75 mm grid and a larger 225 mm grid. All cascade measurements shown here were made in the mid-plane of a gap.

Figure 1 showed an example with the Reynolds stresses non-dimensionalized by the mean free-stream speed. Figure 10 shows the results as ratios $\overline{u_1^2}/\overline{u_{1\infty}^2}$, $\overline{u_2^2}/\overline{u_{2\infty}^2}$ and $\overline{u_3^2}/\overline{u_{3\infty}^2}$ measured at a number of stations with and without a cascade in the flow, the free-stream values being measured at the same x_1 stations. A strong reduction in $\overline{u_3^2}$ is found downstream of each cascade and this reduction is found to persist as far downstream as measurements were taken with, at most, a rather slow return back towards isotropy. The value of $\overline{u_3^2}$ does not tend to zero in the wake plane as the theory would predict, owing at least in part to the large mean shear production in the boundary layers and wakes. $\overline{u_1^2}$ and $\overline{u_2^2}$ show smaller reductions which similarly persist downstream. The anisotropy tensor component $a_{33} = \overline{u_3^2}/\kappa - \frac{2}{3}$ is also plotted in this figure.

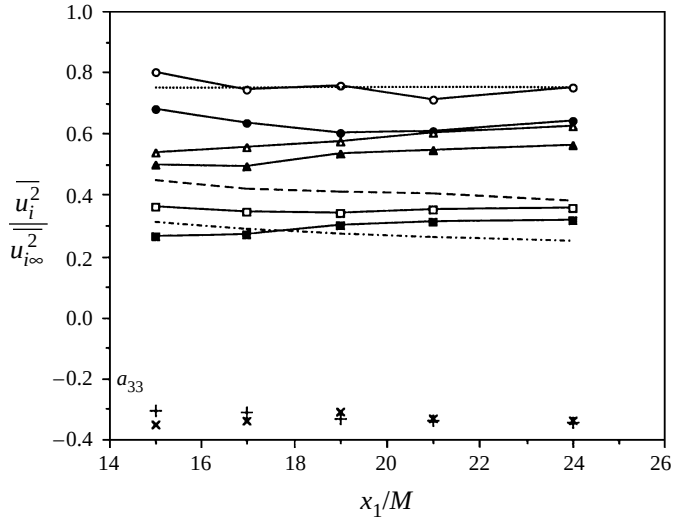

FIGURE 10. $\overline{u_1^2}/\overline{u_{1\infty}^2}$, $\overline{u_2^2}/\overline{u_{2\infty}^2}$, $\overline{u_3^2}/\overline{u_{3\infty}^2}$ measured on the mid-plane behind a cascade. Cascade 1 (NACA0015, $h/c = 0.57$): ○, $\overline{u_1^2}$; △, $\overline{u_2^2}$; □, $\overline{u_3^2}$; ———, RDT; +, a_{33}. Cascade 2 (NACA0008, $h/c = 0.25$): ●, $\overline{u_1^2}$; ▲, $\overline{u_2^2}$; ■, $\overline{u_3^2}$; –·–, RDT; ×, a_{33}. ·····, $\overline{u_1^2}$ RDT ($h/L_\infty = 0$).

x_1/M	h/L_∞ (1)	h/L_∞ (2)
15	0.73	0.41
17	0.68	0.38
19	0.65	0.36
21	0.63	0.35
24	0.59	0.33

TABLE 1. The ratios of h/L_∞ for the two cascade cases

The ratios of h/L_∞ for the two cascade cases (1 and 2) decrease slowly over the x_1 measurement range as L_∞ grows (table 1). The theoretically predicted values of $\overline{u_3^2}/\overline{u_{3\infty}^2}$, assuming that it is appropriate to use the local value of h/L_∞, are also shown in figure 10. The zero gap case predicts that $\overline{u_1^2}/\overline{u_{1\infty}^2}$ and $\overline{u_2^2}/\overline{u_{2\infty}^2}$ should both take the value 0.75 downstream of the cascades. The measured values, particularly of $\overline{u_2^2}$, are somewhat lower, whereas the small non-zero gap values would be predicted to be slightly higher. The value of $\overline{u_3^2}/\overline{u_{3\infty}^2}$ measured in the plane of a plate was larger, probably because of the large production of turbulence in the boundary-layer wake region and effects of leading-edge distortion.

Spectra of u_1, u_2 and u_3 taken in the mid-planes of the gaps are shown in figures 11, 12 and 13. In figure 11, the measured data are compared with the theoretical results for Θ_{11} for infinitesimal gap. Figure 12 shows similar results for the spectrum of the transverse component, Θ_{22}. The low-frequency asymptote for the Θ_{22} spectrum is predicted by RDT to be proportional to k_1. The measured data have much higher values of Θ_{22} at low frequency. However, the Θ_{22} spectrum predicted by RDT is sensitive at the low-frequency end both to gap size and to distance from the plane of a plate. Figure 12 also shows the predicted spectra for the same gap size ($h/L_\infty = 0.6$) as the measurements in both a mid-plane ($x_3' = \frac{1}{2}h$) and in a plate plane ($x_3' = 0$). The low-frequency end of the spectrum is not greatly changed by gap size in the mid-plane but increasing gap size significantly increases $\Theta_{22}(k_1 \to 0)$ in the plane of a plate. The

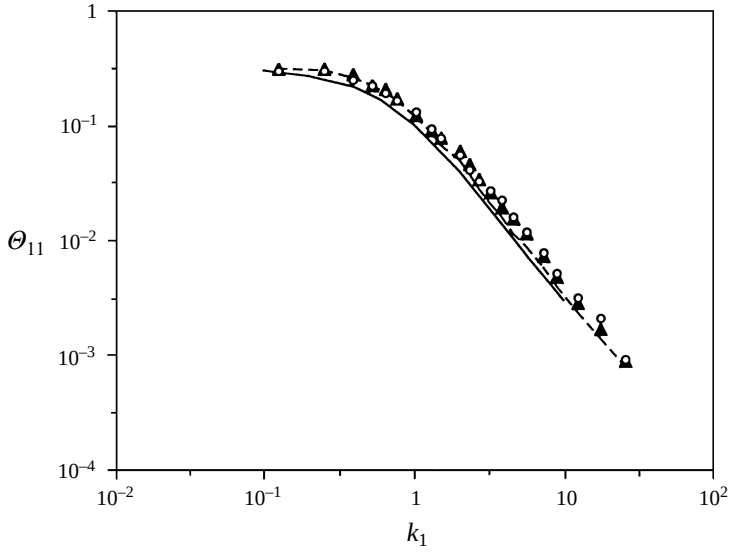

FIGURE 11. Measured and theoretical spectra Θ_{11}, $\Theta_{11\infty}$ downstream of a cascade. ▲, Θ_{11} measured $h/L_\infty = 0.6$, $x_1/M = 13.6$, ——, RDT theory, $h/L_\infty = 0$; ○, $\Theta_{11\infty}$ measured, $x_1/M = 13.6$; – – –, Von Kármán spectrum.

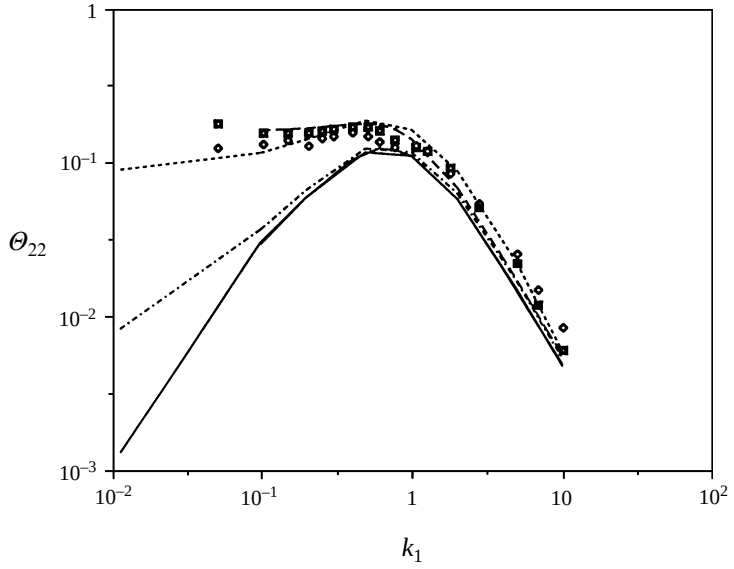

FIGURE 12. Measured and theoretical spectra Θ_{22}, $\Theta_{22\infty}$ downstream of a cascade. ◇, Θ_{22} measured $h/L_\infty = 0.6$, $x_1/M = 13.6$; ——, RDT ($h/L_\infty = 0$); –·–, RDT ($h/L_\infty = 0.6$, $x_3'/h = 0.5$), – – –, RDT ($h/L_\infty = 0.6$, $x_3'/h = 0$); □, $\Theta_{22\infty}$ measured, $x_1/M = 13.6$; – – –, Von Kármán spectrum.

measured results agree much better with the latter although they were measured in a mid-plane downstream of the cascade. This may be due to effects of turbulent diffusion between the mid- and plate planes or to some other unaccounted disturbance. The difference between the low-frequency Θ_{22} spectra at $x_3' = 0$ and $x_3' = \frac{1}{2}h$ is indicative that the contribution from the turbulence to the u_2 component at low frequency downstream comes primarily from long streamwise eddies lying between the plate planes.

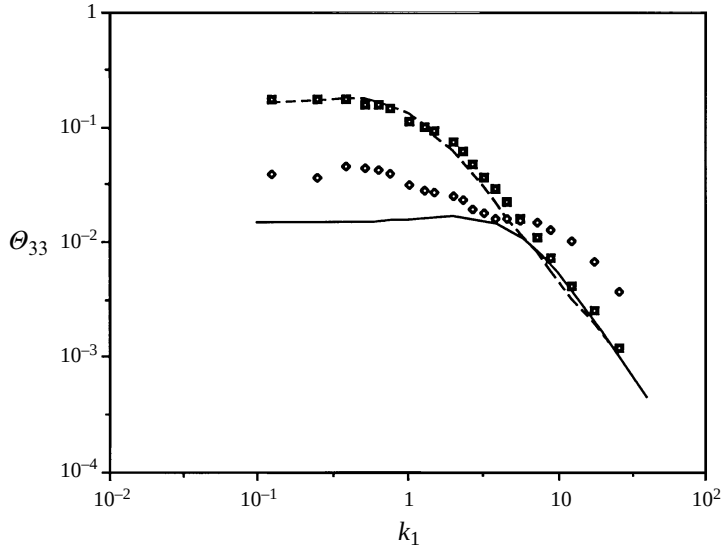

FIGURE 13. Measured and theoretical spectra Θ_{33}, $\Theta_{33\infty}$ downstream of a cascade. $\diamond$, Θ_{33} measured $h/L_\infty = 0.6$, $x_1/M = 13.6$, ——, RDT ($h/L_\infty = 0.6$, $x_3'/h = 0.5$); $\square$, $\Theta_{33\infty}$ measured, $x_1/M = 13.6$; – – –, Von Kármán spectrum.

In the case of the component normal to the cascade plates the theory for the infinitessimal gap gives $\Theta_{33} = 0$ and the measurements for this case which is similarly very sensitive to gap size (figure 9) are compared with the mid-gap theoretical result for the corresponding finite gap. In each case, the measured spectrum at the low-frequency end is distorted in the same way qualitatively, but by a smaller amount than is predicted by the theory, away from the corresponding spectrum for the undisturbed turbulence. At the high-frequency end, the spectra all show evidence of additional production of small-scale turbulence. This degree of increase is not similarly seen in the moving wall data (Thomas & Hancock 1977) and is attributed to the boundary layer and wake turbulence production being distributed, by turbulent diffusion, over the whole flow width downstream so that it is also seen in the mid-plane.

8. Discussion

In the absence of the vortex sheets shed from the trailing edges of the plates the turbulence would undergo a second rapid distortion as it left the plate and the wall boundary condition was removed. This would tend to reverse the leading-edge distortion and restore the status quo except for the residual viscous and nonlinear effects. Because of the Kutta–Joukowski condition, a trailing vortex sheet wake is shed so that flow off a streamwise plate is not the reverse of flow onto the plate. The strength of the two components of the vortex sheet (γ_1, γ_2) can be calculated from the x_2 and x_1 derivatives of the discontinuity in potential at the trailing edge (equation (11)). For each wavenumber $\boldsymbol{k}$ and finite h this is:

$$(\gamma_1, \gamma_2) = \frac{(2\mathrm{i}k_2, -2\mathrm{i}k_1)\,(\cosh \tau h - \cos k_3 h)}{\tau \sinh \tau h} \exp(\mathrm{i}(\omega t - k_1 x_1 - k_2 x_2)). \tag{31}$$

The turbulence downstream of the cascade, according to RDT, is therefore composed of these vortex sheets added to the original vorticity of the turbulence.

In the limit as the gap $h \to 0$ and considering the two fields to be completely mixed within an $O(L_\infty)$ distance $(x_1 - c) \gg h$ downstream of the trailing edges, the resulting vorticity is

$$\boldsymbol{\omega} = (\omega_{1\infty}, \omega_{2\infty}, \omega_{3\infty}) + \lim_{h \to 0} (\gamma_1/h, \gamma_2/h, 0)$$
$$= [\mathrm{i}k_3 u_{2\infty} + \mathrm{i}(k_2 k_3^2/\tau^2) u_{3\infty}, \quad -\mathrm{i}k_3 u_{1\infty} - \mathrm{i}(k_1 k_3^2/\tau^2) u_{3\infty}, \quad -\mathrm{i}k_1 u_{2\infty} + \mathrm{i}k_2 u_{1\infty}]. \quad (32)$$

This vorticity field is consistent with the velocity field derived previously, the last component, $\omega_{3\infty}$, being unchanged by the cascade. The result is a change in the enstrophy $\Omega = \frac{1}{2}\overline{\omega_j \omega_j}$, of the turbulence. From equation (32) for wavenumber $\boldsymbol{k}$, the change is:

$$\Delta\Omega = -\tfrac{1}{2}(k^4/\tau^2)\,\overline{u_{3\infty}^2}.$$

This is a reduction in enstrophy owing to the shedding of the vortex sheets by the plates, since according to RDT there is no change of the vorticity in the flow away from the wall due to its blocking action. Even in the limit $h = 0$ for which $u_3^2 = 0$ the turbulence is clearly not two-dimensional since it contains all three components of vorticity but of strength such that the turbulence velocity field is everywhere in the (1, 2) plane, analogous to a general parallel shear flow. Two-dimensional turbulence is realizable experimentally, for instance by generating it in a soap film (Gharib & Derango 1989; Goldburg, Rutgers & Wu 1996). In the present case, spectra of the developed turbulence well downstream of the cascade have not been measured. In the near downstream region, where they have been measured, Θ_{11} and Θ_{22} do not show any sign of the high-wavenumber k^{-3} behaviour found in two-dimensional turbulence. The measurements (figures 1 and 10) of $\overline{u_1^2}$, $\overline{u_2^2}$ and $\overline{u_3^2}$, as far as they have been taken downstream of the cascade, indicate that the return to isotropy is very slow, as has been observed for highly anisotropic turbulence downstream of a contraction (Uberoi 1956). The rate of return of the large scales which have been distorted by the blocking action may, however, be partly masked by the behaviour of the small scales which are generated in the mean shear regions.

Since $u_3 = 0$ in the theoretically predicted downstream turbulence for the zero gap size limit, the transport equation for the component of vorticity ω_3 normal to the plates is:

$$\frac{\partial \omega_3}{\partial t} + U_\infty \frac{\partial \omega_3}{\partial x_1} + u_1 \frac{\partial \omega_3}{\partial x_1} + u_2 \frac{\partial \omega_3}{\partial x_2} = \nu \left(\frac{\partial^2 \omega_3}{\partial x_1^2} + \frac{\partial^2 \omega_3}{\partial x_2^2} + \frac{\partial^2 \omega_3}{\partial x_3^2} \right)$$

with

$$\frac{\partial u_1}{\partial x_1} + \frac{\partial u_2}{\partial x_1} = 0, \quad \omega_3 = \frac{\partial u_2}{\partial x_1} - \frac{\partial u_1}{\partial x_1}.$$

These are the same equations which govern two-dimensional turbulence except for the additional diffusion term $\nu \partial^2 \omega_3 / \partial x_3^2$. The evolution of the turbulence in each (1, 2) plane is therefore similar to a two-dimensional turbulence, the added diffusion giving somewhat the effect of a lower Reynolds number. For turbulence adjacent to an impermeable surface there is a near balance between the 'splats' (inward surface-normal motion converted by the surface into outward tangential spreading) and 'antisplats' (the opposite). This causes the pressure-strain (which would otherwise redistribute energy from the more energetic tangential Reynolds stresses into the less energetic surface-normal stresses) to be small. In the case of a cascade for which the gap is small, a 'splat' on one surface is an 'antisplat' on the opposing surface. In the limit of zero gap, since u_3 is zero, the pressure-strain and turbulent diffusion terms in the

transport equation for $\overline{u_3^2}$ are also zero. Hence, there would be zero growth rate for this Reynolds stress.

The measured spectra show less reduction of the low-wavenumber components than predicted by RDT, which may be due to the finite gap and thickness of the cascade aerofoils and also to their finite chord which limits nonlinear and viscous effects but also limits the effectiveness of the cascade in suppressing u_3. The high-frequency parts of the spectra are significantly raised above the theoretical prediction, largely owing to small-scale production in the mean shear layers which are generated.

The optimum cascade to generate a nearly planar turbulence at a given Reynolds number has not been investigated here. Increasing plate chord increases cascade effectiveness but also increases the overall nonlinear and viscous effects in the flow. Too small a gap similarly increases the viscous effects. Complete suppression of turbulence is only approximately achievable by a high-resistance narrow-gap array, which also reduces u_1^2 directly through viscous resistance more effectively if the cascade has surfaces in both cross-stream directions, i.e. if it is a honeycomb.

9. Conclusions

Results have been obtained based on the assumptions of rapid distortion theory for the effect of passing homogeneous isotropic turbulence through a cascade of thin streamwise plates. Suppression of the transverse component of turbulent velocity normal to the plates is predicted, which should be complete in the limit when the cascade gap to turbulence lengthscale ratio goes to zero. This suppression is predicted to continue downstream of the cascade owing to the vortex sheet wakes which are shed into the downstream flow. The resulting 'planar' turbulence field is analogous to a general plane shear.

Measurements have been made in a wind tunnel of turbulent flow emerging from a cascade, obtained by passing nearly isotropic grid generated turbulence through cascades of thin plates and aerofoils with finite gaps. The cascades are shown to affect the turbulence in a similar way to that predicted by the theory for zero gap. However, the variances of the three velocity components of the turbulence downstream of the cascade are higher than predicted. Part of this is due to the finite gap sizes used in the experiments. Measurements of variances taken behind single and double (biplane) streamwise plates show similar agreement with the theory, with higher levels of turbulence found in the regions of the plate planes. These are probably partly due to production in the boundary- and wake shear layers of the plates and partly due to turbulence having previously passed through the local strain field of a plate leading edge.

Calculation of some of the spectral and variances downstream of a cascade from the theory for finite gap show that the results are very sensitive to gap size, and at the low-frequency end of the spectrum to the position across the gap at which the turbulence is measured. At the high-frequency end neither the measured spectra at moderate distances downstream of the cascade, nor RDT theory, show the faster k^{-3} fall-off in power that is expected for a fully developed two-dimensional turbulence. The stations where the turbulence quantities were measured were downstream of the plate trailing edges and hence always at distances downstream of the onset of distortion (at the leading edges) which are large compared with the lengthscale of the turbulence. At such distances, the distortion has acted on the turbulence for a time which cannot properly be considered to be small compared with the eddy turnover time. Analagous to what has been shown previously for walls and slip surfaces, the normal component of the

turbulence remains suppressed approximately as predicted by RDT over considerable distances but the streamwise and transverse components tend to values above those predicted.

REFERENCES

Aronson, D., Johansson, A. V. & Loefdahl, L. 1997 Shear-flow turbulence near a wall. *J. Fluid Mech.* **338**, 363–385.

Atassi, H. M. & Gebert, G. A. 1987 Modification of turbulent boundary layer structure by large-eddy breakup devices. *Intl Conf. Drag Reduction by Passive Means*, pp. 432–456, Royal Aeronautical Society, London.

Balakumar, P. & Widnall, S. E. 1986 Application of unsteady aerodynamics to large-eddy break-up devices in a turbulent flow. *J. Fluid Mech.* **194**, 479–510.

Basuki, J. 1983 Unsteady flows over aerofoils and cascades. PhD thesis, London University.

Batchelor, G. K. & Proudman, I. 1954 The effect of rapid distortion of a fluid in turbulent motion. *Q. J. Mech. Appl. Maths* **7**, 83–103.

Dowling, A. 1985 The effect of large-eddy break-up on oncoming vorticity. *J. Fluid Mech.* **160**, 447–463.

Gharib, M. & Derango, P. 1989 A liquid film (soap film) tunnel to study two-dimensional laminar and turbulent shear flows. *Physica* **37**D, 406–416.

Gibson, M. M. & Launder, B. E. 1978 Ground effects on pressure fluctuations in the atmospheric boundary layer. *J. Fluid Mech.* **86**, 491–511.

Graham, J. M. R. 1970 Lifting surface theory for the problem of an arbitrarily yawed sinusoidal gust incident on a thin aerofoil in incompressible flow. *Aero. Q.* **21**, 182–198.

Graham, J. M. R. 1975 Turbulent flow past a long flat plate. Imperial College Aero. Tech. Note 75-101.

Goldburg, W. I., Rutgers, M. A. & Wu, X.-I. 1997 Experiments on turbulence in soap films. Physica **239**A, 340–349.

Haidos, C. 1983 Study of turbulence interacting with a cascade. MSc thesis, Imperial College, University of London.

Hunt, J. C. R. 1973 A theory of turbulent flow round two-dimensional bluff bodies. *J. Fluid Mech.* **61**, 625–706.

Hunt, J. C. R. & Graham, J. M. R. 1978 Free stream turbulence near plane boundaries. *J. Fluid Mech.* **84**, 209–235.

Kullar, I. & Graham, J. M. R. 1986 Acoustic effects due to turbulence passing through a cascade of thin aerofoils. *J. Sound Vib.* **110**, 143–160.

Maxey, M. R. 1978 Aspects of unsteady turbulent shear flow, turbulent diffusion and tidal dispersion. PhD thesis, University of Cambridge.

Perot, B. & Moin, P. 1995 Shear-free turbulent boundary layers. Part 1. Physical insights into near-wall turbulence. *J. Fluid Mech.* **295**, 199–227.

Reissner, E. 1947 Effect of finite span on the airload distributions for oscillating wings. NACA Tech. Note 1194.

Saxena, V. 1994 Turbulence distortion around leading edges and its effect on boundary layers. PhD thesis, University of Cambridge.

Thomas, N. H. & Hancock, P. E. 1977 Grid turbulence near a moving wall. *J. Fluid Mech.* **82**, 481–496.

Uberoi, M. S. 1956 Effects of wind tunnel contraction on free stream turbulence. *J. Aero. Sci.* **23**, 754–764.

Uzkan, T. & Reynolds, W. C. 1967 A shear-free turbulent boundary layer. *J. Fluid Mech.* **28**, 803–821.

Walker, D. T., Leighton, R. I. & Garza-Rios, L. O. 1996 Shear free turbulence near a flat free surface. *J. Fluid Mech.* **320**, 19–51.